In situ measurements of Raman scattering in clear ocean water

Chuanmin Hu and Kenneth J. Voss

We have further developed and improved the prototype oceanic Fraunhofer line discriminator by using a well-protected fiber-optic–wire cable and in-water electronic housing. We conducted a series of *in situ* measurements in clear ocean water in the Florida Straits. By comparing the reduced data with the Monte Carlo simulation results, we verify the Raman scattering coefficient B_r with an excitation wavelength at 488 nm to be $2.6 \times 10^{-4}\,\mathrm{m}^{-1}$ [Appl. Opt. **29,** 71–84 (1990)], as opposed to $14.4 \times 10^{-4}\,\mathrm{m}^{-1}$ [Appl. Opt. **14,** 2116–2120 (1975)]. The wavelength dependence of the Raman scattering coefficient is found to have an insignificant effect on the in-water light field. We also discuss factors that lead to errors. This study can be used as a basis for inelastic light scattering in the radiative transfer theory and will allow other inelastic light, e.g., fluorescence, to be detected with *in situ* measurements. © 1997 Optical Society of America

Key words: Raman scattering, inelastic scattering, ocean optics.

1. Introduction: Raman Scattering and the Oceanic Fraunhofer Line Discriminator

Raman scattering in water is caused by the change of the O–H vibrational modes of water molecules[1,2]: an incident photon at a certain frequency is scattered by the molecule and shifted in frequency by 3357 cm^{-1}. Owing to the experimental difficulty, the value reported in the literature for the Raman scattering cross section $[d\sigma(488)/d\Omega]$ varies from 8.1×10^{-30} to $45 \times 10^{-30}\,\mathrm{cm}^2\,\mathrm{sr}^{-1}\,\mathrm{molecule}^{-1}$.[2–5] The dependence of this parameter on the Raman emission wavelength also varies in the literature from λ^{-4} to λ^{-5}.[1,6]

The importance of Raman scattering in the ocean has been addressed by many authors, and various models have been established to simulate the Raman scattering effect on the in-water light field.[3,6–12] However, no direct *in situ* measurement under solar illumination was available to quantify the Raman scattered light and to test the models until recently when the oceanic Fraunhofer line discriminator (OFLD) instrument was developed and *in situ* measurement was made possible.

The idea of using solar Fraunhofer lines to study inelastic light scattering (which is a sum of Raman scattering and fluorescence) is simple but not new. By measuring the change in the absorption line depth of a Fraunhofer line, one can determine the proportion of inelastic light in the total light field. In the 60's Fraunhofer lines were used to study inelastic light scattering in the atmosphere.[13–16] In the 70's Fraunhofer lines were used to study the ocean's reflected fluorescence.[17,18] And more recently instruments such as the Fraunhofer line underwater experiment[19] and the prototype OFLD[20] were used *in situ* in ocean water to study the variation in Fraunhofer line shapes.

The prototype OFLD[20] consisted of a fiber-optic irradiance collector, a single large fiber (1-mm core size), and a 1-m-focal-length monochromator. The spectral resolution was approximately 0.008 nm, which was sufficient to resolve the 0.1-nm Fraunhofer lines. A CCD array was placed on the focal plane of the monochromator to collect the entire Fraunhofer line and surrounding spectrum (~3 nm) simultaneously. We made several modifications that are now described. We replaced the single fiber used previously with a fiber–wire cable. This cable has eight multimode, all-silica, 100-μm-core-size fibers protected by a metal shield and eight wire conductors. The cable is 150 m long: 20 m is for on-ship operation, leaving 130 m for in-water use. We built an in-water case to house the fiber splice for two cosine irradiance fiber collectors, a depth transducer,

two cosine irradiance photocell collectors, and the electronic boards for power supply and signal transmission. The depth transducer measures depth to an accuracy of ± 0.1 m through the operation range. The photocell collectors are used to monitor the wideband downwelling and upwelling light levels. Neutral-density and interference filters are used to choose the appropriate signal range and wavelength. All the electronic devices are powered and controlled by an electronic control box that has three digital readout boards to read the depth and photocell sensors.

Eight fibers are used to transmit light collected by the downwelling and upwelling cosine irradiance collectors, with four fibers in each. A fiber–wire splice box is used to separate the channels. Six fibers, arranged in a linear array (three from downwelling and three from upwelling), are built into the fiber ferrule. The remaining two fibers are designed to measure the spectra through the whole visible band but are currently unused. The fiber array is placed at the entrance slit of the monochromator and imaged on the CCD array at the output of the monochromator. Thus six tracks on the CCD are used to record the signal from the corresponding six fibers. Other components of the system are as described previously.[20] With appropriate adjustment and alignment the system can achieve ~4000 counts/second/pixel on the CCD under normal solar illumination (~100 μw cm^{-2} nm^{-1} in the visible band). The total spectral width measured in one image is a weak function of wavelength and is ~3 nm for the 512 data points on the CCD.

2. Data Reduction Procedures

As described above,[21] a parameter with an equivalent width w is used to describe the Fraunhofer line size. It is defined as

$$w = \int_{\lambda_1}^{\lambda_2} \left[1 - \frac{E(\lambda)}{E_b(\lambda)} \right] d\lambda, \qquad (1)$$

where $E(\lambda)$ is the spectral irradiance and λ_1 and λ_2 are the starting and ending points of the Fraunhofer line. $E_b(\lambda)$ is the background irradiance, which is a straight line formed by $E(\lambda_1)$ and $E(\lambda_2)$. At depth z the ratio of inelastically scattered irradiance to total irradiance, and the ratio of direct transmitted and elastically scattered irradiance to total irradiance, can be shown to be

$$\frac{E_{\mathrm{in}}(z)}{E_t(z)} = \left[1 - \frac{w(z)}{w_0} \right], \qquad (2)$$

$$E_{\mathrm{el}}/E_t = \frac{w(z)}{w_0}, \qquad (3)$$

respectively, where $w(z)$ and w_0 are equivalent widths at depth z and the surface, respectively. We have found that the normalized equivalent width [i.e., $w(z)/w_0$] does not depend strongly on the choice

of λ_1 and λ_2. [Varying λ_1 or λ_2 by 0.5 nm changes $w(z)/w_0$ by $<2\%$.]

To reduce w effectively, one must remove the dark current from the measured spectrum. Since the dark current is not homogeneous on the CCD array because of a temperature gradient on the array, the six tracks used to measure the signal are also used to measure the dark current. In addition, two extra tracks are used to record the stray light in the system. Thus the dark current and the stray light can be removed from the spectrum by application of simple algebra.

The spectrum has units of counts versus CCD pixels. Wavelength calibration is needed to convert each pixel to the corresponding wavelength. This is done by using a standard high-spectral-resolution solar atlas[22] to identify the wavelengths visually for two absorption peaks in the spectrum. A linear calibration is then applied to convert the pixels to wavelengths.

Although the new OFLD is superior to its predecessor in several ways, there is one trade-off as well. The small-core-size fibers reduce the light that enters the monochromator to approximately one fifth of the old system. Thus noisy spectra are obtained in deep waters and for long wavelengths. Therefore a fitting procedure is used to clean the noisy spectra (Fig. 1). A reference spectrum (usually measured at the surface) is used as a template to fit the noisy spectrum by use of a least-squares fit. The wavelength dependence of the water transmittance is assumed to be linear within the 3-nm bandwidth. Thus the functional form of the fitting formula is given by

$$f(\lambda) = Ay_0(\lambda) + B\lambda + C, \qquad (4)$$

where $y_0(\lambda)$ is the reference spectrum [Fig. 1(a), curve I] and fitting coefficients A, B, and C account for wavelength-independent transmission, wavelength-dependent transmission, and line filling, respectively. Using $f(\lambda)$, one can use a least-squares fit to the data at depth $y_z(\lambda)$ [Fig. 1(a), curve II] to obtain a clean spectrum $y_z^{\mathrm{fit}}(\lambda)$ [Fig. 1(b), curve II]. The depth spectrum is sometimes wavelength shifted from the reference line owing to the monochromator scan error [Fig. 1(a), curve II], and this shift can be as much as 25 data points (~0.2 nm). To correct this shift error, one must shift the data point by point and compare them to the surface template. An error for each shift is determined by

$$Q_n = \sum_{\lambda} \left[f(\lambda) - y_{z,n}(\lambda) \right]^2, \qquad (5)$$

where n is the number of shifted data points. Comparing the Q_n for n from -30 to 30, we obtain the least Q at $n = n_0$, thus determining the correct offset. To reduce the error caused by stray light, we cut 100 data points at each end of the spectra before the fit [Fig. 1(b), curve II]. Since these data points are out of the integration limits in Eq. (1), there is no effect on w.
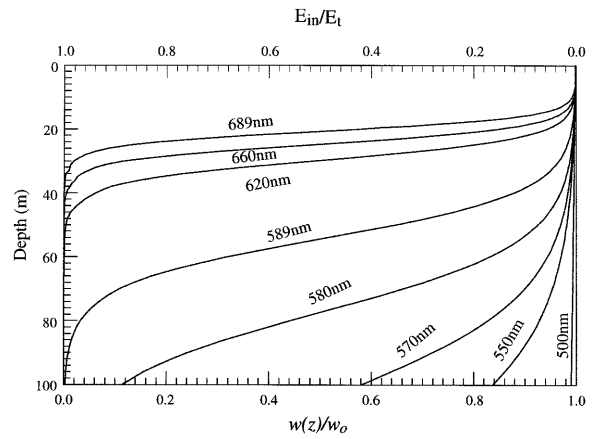
The fitting procedure has three advantages.
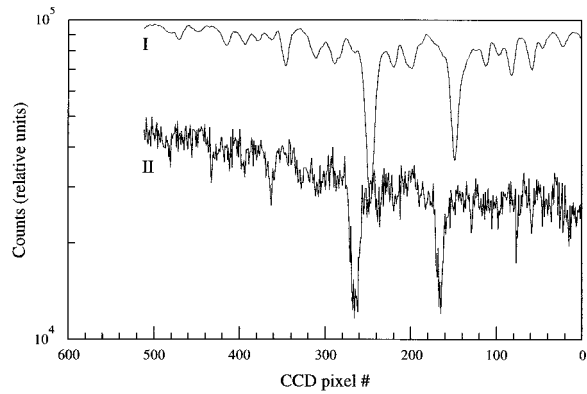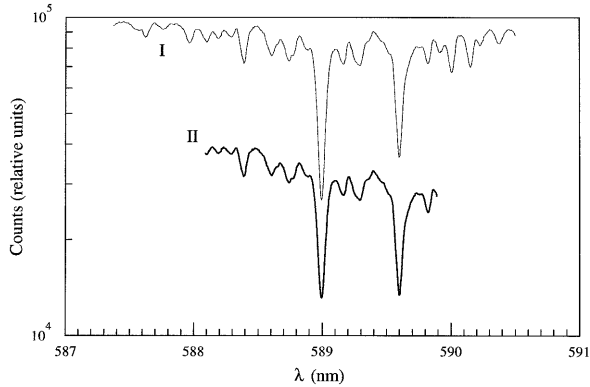
Fig. 1. Raw data and fitted spectrum using the fitting procedure. (a) I, surface reference spectrum $y_0(\lambda)$ as the template; curve II, depth spectrum $y_z(\lambda)$, which is noisy and data pixel shifted. (b) A fitted, clean, and shift-corrected spectrum II $[y_z^{fit}(\lambda)]$ obtained by use of I $[y_0(\lambda)]$ as the template to least-squares fit the noisy spectrum.

Fig. 2. From the Monte Carlo simulation normalized equivalent width $[w(z)/w_0]$ is obtained as a function of depth and wavelength. The ratio of inelastic light over total light (E_{in}/E_t) is $1 - w(z)/w_0$. (a) Downwelling data; (b) upwelling data. In the simulation the sky is clear and the optical thickness of aerosol at 550 nm is 0.25. The solar zenith angle is 25°, and the wind speed is 5 m/s. Pigment concentration is 0.1 mg/m^3 throughout the water column.
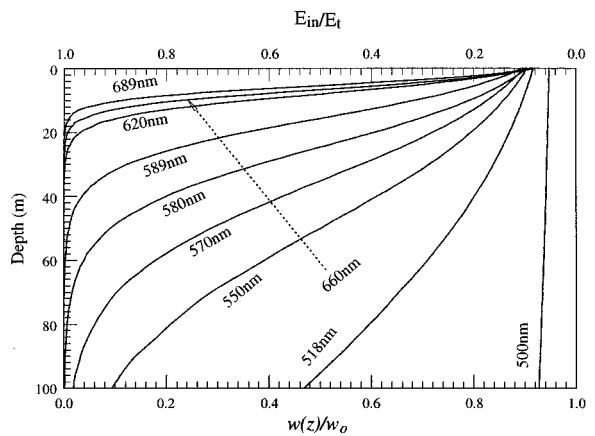
First, it allows wavelength calibration of each data spectrum. When the spectrum is noisy visual identification of a specific spectral feature is impossible, so use of a standard solar atlas is not feasible. Second, it enables the correct background (for computation of w) to be determined for a noisy spectrum. w strongly depends on the background, which is a straight line formed by the two spectral points at λ_1 and λ_2. Large errors can occur if the background is chosen from the noisy spectrum. Finally, the fitting procedure can minimize the effect of sky variation on the measurement, as we describe below.

3. Theory Review and Monte Carlo Simulation

Various models have been established to simulate Raman scattering in seawater.[8,10–12] Here we choose the one used by Ge *et al.*[11] Only a small correction is made to modify the radiative transfer in the atmosphere. In this Monte Carlo code the in-water irradiance $E(\lambda)$ is normalized to unit irradiance entering the top of the atmosphere, then multiplied by the extraterrestrial solar irradiance $F_0(\lambda)$ to provide the actual irradiance. The in-water irradiance profiles at both excitation wavelength λ_{ex} and emis-

sion wavelength λ_{em} are simulated separately. The Rayleigh scattering cross section of air molecules, absorption coefficient for pure O_3, and aerosol attenuation coefficient are all functions of λ, and the parameters used were published by Elterman.[23] The simulation results are slightly different from those of Ge *et al.*[11]

Simulation results of Raman scattering from 500 to 700 nm are presented here to illustrate the percentage of Raman scattered light in the total light field to as low as 100 m for both downwelling and upwelling irradiances (Fig. 2). Data for wavelengths below 500 nm are not presented here because the light field contains virtually no inelastic light from 400 to 500 nm. In the simulation the sky is clear, the optical thickness of aerosol is 0.25 at 550 nm, the solar zenith angle is 25°, the wind speed is 5 m/s, and the pigment concentration is 0.1 mg/m^3 throughout the water column. Other inputs are as described previously.[11] These figures clearly show how the light field is af-
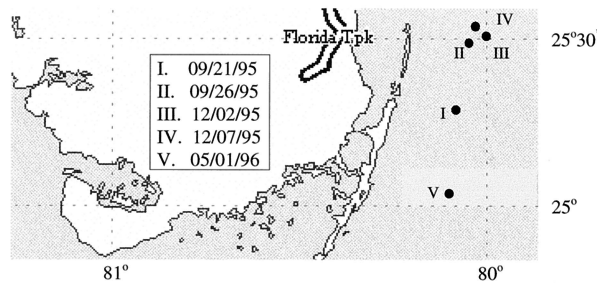
Fig. 3. Station locations in the Florida Straits.

Fig. 4. Normalized equivalent width $[w(z)/w_0]$ for the Fraunhofer line at 589 nm for both downwelling and upwelling. The simulation uses the pigment concentration, wind speed, and solar zenith angle data from the 7 December 1995 station. Only Raman scattering is considered in the model with the excitation at 491 nm. Three different Raman scattering coefficients B_r are used in the model.

fected by Raman scattering as a function of wavelength and depth. For example, Raman scattering is more significant in the upwelling light field than in the downwelling light field for all wavelengths and depths studied. The proportion of Raman scattered light in the total light field (E_{in}/E_t) increases with both wavelength and depth. In the downwelling light field, from 570 to 620 nm, the profile of E_{in}/E_t versus depth changes drastically. In the upwelling light field, however, the large change occurs between 500 and 550 nm. In the band 620–689 nm the profile is a relatively weak function of wavelength for both downwelling and upwelling light fields, and the upwelling light contains significant Raman scattered light even in the surface water [Fig. 2(b)].

4. Data Acquisition

The study reported here took place on three cruises in 1995 and 1996 on the research ship, RV (research vessel) Calanus (Fig. 3). Pigment data collected at several of the stations[24] indicated that the pigment concentration was less than 0.1 mg/m³. In general the water was clear. The solar zenith angle was approximately 30° in the summer and 50° in the winter during the data collection. Wind speed was ~5 m/s. Care was taken to collect the data only when the sky was clear and the detector head was not in the ship's shadow. Also the measurements were taken within ±3 h of solar noon to make sure that the surface Fraunhofer line was stable. We performed laboratory tests to determine the optimal CCD exposure time by using neutral-density filters to simulate the low light level in deep water and in the red. It was found that the maximum effective exposure time is 120 s. The deepest measurement depth is limited by the light level and the cable length and is given in Table 1 for the Fraunhofer line wavelengths.

Table 1. Depths of the OFLD Detector can Reach[a]

λ_f(nm)	434.05 Down/Up	486.13 Down/Up	518.36 Down/Up	589.00 Down/Up	656.28 Down/Up
Depth (m)	70/50	130/70	120/55	55/18	20/4

[a]Depths were limited by light level and cable length for both downwelling and upwelling. These are typical values for summer in the clear water of the Florida Straits.
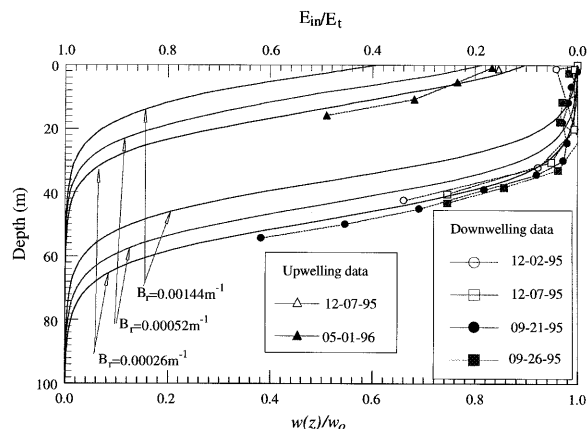
5. Results and Discussion

At short wavelengths (434 and 486 nm), Raman scattering was found to be negligible in both downwelling and upwelling light fields at all depths that we could measure. At 518 nm, although the situation is the same for downwelling light, below 25 m the upwelling light contains >20% Raman scattered light. Thus in clear ocean water Raman scattering can generally be neglected in the blue region. However, in the yellow (589-nm) and red (656-nm) regions the Raman scattered light occupies a considerable portion in the total light field.

In Fig. 4 the fraction of inelastically scattered light in the total light field for both downwelling and upwelling is drawn versus depth. It is easy to see that the data are fairly stable from station to station, although a small difference caused by the change of solar zenith angle does exist between summer and winter data. At ~50 m, 50% of the downwelling light is from Raman scattering. For upwelling light this depth is ~18 m. In the Monte Carlo simulation environmental data (solar zenith angle, wind speed, and pigment concentration) from the 7 December 1995 station were used to simulate the light fields. The key parameter in the code is the Raman scattering coefficient B_r. When Marshall and Smith's value of 2.6×10^{-4} m^{-1} was used, good agreement was found between the simulation results and the experimental data. Other values of B_r from the literature show little agreement between the model and the experiment. Thus this result confirms the B_r measurement of Marshall and Smith.[3]

Similar results for the light fields at 656 nm are presented in Fig. 5. Although all the data sets are stable for different stations at 589 nm, the downwelling data from the 21 September 1995 station at 656 nm obviously diverge from others and show a larger inelastic component than Raman scattering
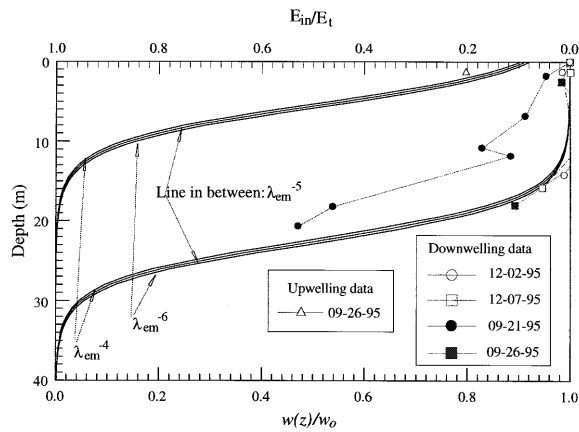
Fig. 5. Normalized equivalent width $[w(z)/w_0]$ for the Fraunhofer line at 656 nm for both downwelling and upwelling. The simulation uses the pigment concentration, wind speed, and solar zenith angle data from the 7 December 1995 station; the λ_{em}^{-5} dependence of the Raman scattering coefficient in the model is assumed to be λ_{em}^{-4}, λ_{em}^{-5} and λ_{em}^{-6}, respectively.

alone. We suspect this is from chlorophyll-a fluorescence since 656 nm is on the edge of the chlorophyll-fluorescence emission band. Unfortunately, pigment concentration data are not available for this station, so we cannot verify this conjecture. Since the B_r dependence on Raman emission wavelength λ_{em} varies in the literature[6,7] from λ_{em}^{-4} to λ_{em}^{-5}, we used three values, namely, λ_{em}^{-4}, λ_{em}^{-5}, and λ_{em}^{-6}, in the simulation. Negligible difference is found among the results. Simulations at other wavelengths yield the same results. Thus the wavelength dependence is not critical in simulating the naturally occurring Raman scattered light in water, owing to the limited wavelength range encountered.

Because of the sky condition variation and the procedures used to reduce the data, errors can exist in the equivalent width computation. The effect of sky variation on the Fraunhofer line as a function of local time is one source of error. We made a series of measurements of the downwelling irradiance Fraunhofer lines in different seasons and sky conditions from early morning to late afternoon and found a variation in the equivalent width that could be explained by water vapor absorption at ~589 and 656 nm.[25] With the fitting procedure used, variations in the small shoulders around the Fraunhofer line can be filtered out, reducing errors caused by sky variation. The conclusion from the above measurements is that, with reasonable care and measurements within ±3 h of local noon, the reduced surface-equivalent width generally has a relative error of <2%.

Estimates of the error involved in the fitting procedure to compute the equivalent width were also determined. Neutral-density filters were used to make the spectrum noisy. Then we produced artificial filling by adding a constant background to the spectrum. The fitting procedure was applied to the spectrum, and the error of the calculated equivalent

width was determined. It was concluded that the maximum error in the procedure is ~5% for noisy spectra.

With other factors on a cruise, such as instrument frame shadow or cable shadow, for the deep-water noisy spectra the maximum error in reduced equivalent width is estimated to be <10%.

6. Conclusion

For the first time, to our knowledge, the Raman scattering coefficient has been verified in real ocean water under normal solar illumination. This result, combined with the state-of-the-art instrumentation of the OFLD and data-reduction procedures, will be used as the basis for extracting other inelastic components, such as chlorophyll fluorescence, in the total measured inelastic light.

References

1. A. Anderson, *The Raman Effect: Principles*, (Dekker, New York, 1971), Vol. 1.
2. R. B. Slusher and V. E. Derr, "Temperature dependence and cross sections of some Stokes and anti-Stokes Raman lines in ice Ih," Appl. Opt. **14**, 2116–2120 (1975).
3. B. R. Marshall and R. C. Smith, "Raman scattering and in-water ocean optical properties," Appl. Opt. **29**, 71–84 (1990).
4. I. I. Kondilenko, P. A. Korotkov, V. A. Klimenko, and O. P. Demyanenko, "Transverse cross section of Raman scattering of the v_1 vibration of the water molecule in the liquid and gaseous state," Opt. Spectrosc. (USSR) **43**, 384–386 (1977).
5. N. P. Romanov and V. S. Shuklin, "Raman scattering cross section of liquid water," Opt. Spectrosc. (USSR) **38**, 646–648 (1975).
6. S. Sugihara, M. Kishino, and N. Okami, "Contribution of Raman scattering to upward irradiance in the sea," J. Oceanogr. Soc. Jpn. **40**, 397–404 (1984).
7. F. E. Hoge and R. N. Swift, "Airborne simultaneous spectroscopic detection of laser-induced water Raman backscatter and fluorescence from chlorophyll a and other naturally occurring pigments," Appl. Opt. **20**, 3197–3205 (1981).
8. R. H. Stavn and A. D. Weidemann, "Optical modeling of clear ocean light fields: Raman scattering effects," Appl. Opt. **27**, 4001–4011 (1988).
9. R. H. Stavn, "Raman scattering effects at the shorter visible wavelengths in clear ocean water," in *Ocean Optics* X, R. W. Spinrad, ed., Proc. SPIE **1302**, 94–100 (1990).
10. G. W. Kattawar and X. Xu, "Filling in of Fraunhofer lines in the ocean by Raman scattering," Appl. Opt. **31**, 6491–6500 (1992).
11. Y. Ge, H. R. Gordon, and K. J. Voss, "Simulation of inelastic-scattering contributions to the irradiance field in the ocean: variation in Fraunhofer line depths," Appl. Opt. **32**, 4028–4036 (1993).
12. V. I. Haltrin and G. W. Kattawar, "Self-consistant solutions to

the equation of transfer with elastic and inelastic scattering in oceanic optics: I. Model," Appl. Opt. **32,** 5356–5367 (1993).

13. J. F. Grainger and J. Ring, "Anomalous Fraunhofer line profiles," Nature (London) **193,** 762 (1962).

14. J. Noxon and R. Goody, "Noncoherent scattering of skylight," Izv. Atmos. Ocean. Phys. **1,** 163–166 (1965).

15. F. E. Barmore, "The filling-in of Fraunhofer lines in the day sky," J. Atmos. Sci. **32,** 1489–1493 (1975).

16. M. Conde, P. Greet, and F. Jacka, "The ring effect in the sodium D2 Fraunhofer line of day skylight," J. Geophys. Res. **97,** 11561–11565 (1992).

17. G. E. Stoertz and W. R. Hemphill, "Airborne fluorometer applicable to marine and estuarine studies," Mar. Technol. Soc. J. **3,** 11–26 (1969).

18. J. A. Plascyk, "The MK II Fraunhofer line discriminator (FLD-II) for airborne and orbital remote sensing of solar-stimulated luminescence," Opt. Eng. **14,** 339–346 (1975).

19. M. G. Lovern, M. W. Roberts, S. A. Miller, and G. T. Kaye, "Oceanic *in situ* Fraunhofer line characterizations," in *Ocean Optics* XI, G. D. Gilbert, ed., Proc. SPIE **1750,** 149–160 (1992).

20. Y. Ge, K. J. Voss, and H. R. Gordon, "Measurement of oceanic inelastic scattering using solar Fraunhofer lines," in *Ocean Optics* XI, G. D. Gilbert, ed., Proc. SPIE **1750,** 161–169 (1992).

21. C. Hu and K. J. Voss, "Solar-stimulated inelastic light in clear sea water," in *Ocean Optics* XIII S. G. Ackleson, ed., Proc. SPIE **2963,** 266–271 (1997).

22. J. M. Beckers, C. A. Bridges, and L. B. Gilliam, "A high resolution spectral atlas of the solar irradiance from 380 to 700 nanometers. Volume II: graphical form," AFGL-TR-76-0126, Environmental Research Paper **565,** (Air Force Geophysics Laboratory, Hanscom Air Force Base, Mass., 1976).

23. L. Elterman, "UV, visible, and IR attenuation for altitudes to 50 km, 1968," AFCRL-68-0153, Environmental Research Paper **285,** (Air Force Cambridge Research Laboratory, Bedford, Mass., 1968).

24. R. G. Zika, C. A. Moore, and C. Farmer, Rosenstiel School of Marine and Atmospheric Science, University of Miami, 4600 Rickenbacker Causeway, Miami, Fla. 33149 (personal communication, 1996).

25. H. R. Gordon, "Radiative transfer in the atmosphere for correction of ocean color remote sensors," in *Ocean Colour: Theory and Applications in a Decade of CZCS Experience*, V. Barale and P. M. Schlittenhardt, eds. (ECSC, EEC, EAEC, Brussels, 1993), pp. 33–77.